Steel and Composite Structures, *Vol. 18, No. 5 (2015) 1161-1176*
DOI: http://dx.doi.org/10.12989/scs.2015.18.5.1161

Energy dissipation of steel-polymer composite beam-column connector

Yun-Che Wang * and Chih-Chin Ko

Department of Civil Engineering, National Cheng Kung University, Tainan 70101, Taiwan

(*Received July 01, 2013, Revised October 18, 2014, Accepted November 10, 2014*)

Abstract. The connection between a column and a beam is of particular importance to ensure the safety of civil engineering structures, such as high-rise buildings and bridges. While the connector must bear sufficient force for load transmission, increase of its ductility, toughness and damping may greatly enhance the overall safety of the structures. In this work, a composite beam-column connector is proposed and analyzed with the finite element method, including effects of elasticity, linear viscoelasticity, plasticity, as well as geometric nonlinearity. The composite connector consists of three parts: (1) soft steel; (2) polymer; and (3) conventional steel to be connected to beam and column. It is found that even in the linear range, the energy dissipation capacity of the composite connector is largely enhanced by the polymer material. Since the soft steel exhibits low yield stress and high ductility, hence under large deformation the soft steel has the plastic deformation to give rise to unique energy dissipation. With suitable geometric design, the connector may be tuned to exhibit different strengths and energy dissipation capabilities for real-world applications.

Keywords: beam-column connector; soft steel; polymer; composite material; energy dissipation

1. Introduction

High damping and high stiffness materials are crucial in energy dissipation applications for increasing seismic resistance or reducing undesired vibrations (Symans *et al*. 2008, Lakes 2009). Among available energy dissipation systems for seismic applications, Symans *et al*. (2008) listed viscous fluid dampers, viscoelastic dampers, metallic dampers and friction dampers as well as widely used passive damping elements. It is noted that the failure of the beam-column connector in steel structures is one of important failure modes (Taranath 1988). Hence, the connection between a column and a beam is of particular importance to ensure the safety of civil engineering structures, such as high-rise buildings and bridges (Higashino and Okamoto 2006, Kappos 2012, Zhang and Wang 2012). The role of the connector is to transmit loading from the beam to the column, and then through the columns to the foundation of the structure. Conventional methods to connect the beam and column use bolts or welding techniques (Calado *et al*. 2013). These methods may give rise to enough rigidity to the connector, and hence it can sustain the large loading. However, at the same time, bolts and welds make the connector brittle, and the brittleness reduces the energy

*Corresponding author, Associate Professor, E-mail: yunche@mail.ncku.edu.tw

http://www.techno-press.org/?journal=scs&subpage=8 ISSN: 1229-9367 (Print), 1598-6233 (Online)

dissipation of the connector in the steel structures.

In the literature, Chen *et al*. (1996) proposed a cross-section area reduction method to enhance the ductility of the beam-column connector. The ductile connectors may localize failure to the beams, and protect the columns. While the connector must bear sufficient force for load transmission, increase of its ductility, toughness and damping may greatly enhance the overall safety of the structure. Yet, current popular designs, such as the cross-section area reduction method, may have limited benefits, in terms of ductility and toughness, to the overall behavior of the beam-column system. Similar design concepts have been realized in creating energy-absorbing devices (Kelly *et al*. 1972, Whittaker *et al*. 1991, Tsai *et al*. 1993). All these ideas and devices do not take the advantages of composite materials with a high-damping phase.

In addition to structure-like damper devices or mass damper devices, several novel dampers have been proposed. In the case of using viscous fluids, compound lead extrusion magnetorheological (CLEMR) dampers have recently been studied for their high energy dissipation properties (Xu *et al*. 2012, Zhang and Xu 2012). In addition, effective damping can be largely enhanced by using negative stiffness elements (Dong and Lakes 2012). Both of the types of the dampers require additional design considerations for real-world applications, in terms of stability and operational frequency ranges. Furthermore, buckling-restrained systems, as a type of metallic dampers, have also been largely adopted into structures to enhance overall damping of the structures (Tremblay *et al*. 2006).

In this paper, a composite beam-column connector, consisting viscoelastic material and low-yield steel, is proposed to behave as an energy dissipation device, and simultaneously allow ductile behavior at the beam-column joint. Composites comprising polymers and metallic materials are widely used in damping applications. Typically, constrained layer dampers have been shown to be an effective method to obtain high damping and sufficient stiffness (Ross *et al*. 1959, Nashif *et al*. 1985, Ferreira *et al*. 2013). The basic idea is to combine high loss material as one phase with high stiffness material as the other phase. The two phase viscoelastic composites have been shown to exhibit desired combination of stiffness and energy dissipation properties.

Along this line of research, Ibrahim *et al*. (2007) proposed a visco-plastic device, as an add-on device consisting of steel plates and viscoelastic material, to increase the energy dissipation capacity of structures. Similarly, Kim *et al*. (2006) studied the effects of viscoelastic dampers for their seismic performance evaluation on structures. Recently, usage of viscoelastic material in a multi-dimensional earthquake isolation device for reticulated structures have been conducted, and the efficacy of viscoelastic material in energy dissipation is evaluated (Xu *et al*. 2013). Moreover, Zou *et al*. (2013) studied the vibration isolation capability of viscoelastic material under a prestressed state. In order to better quantify viscoelastic materials, some detailed parameter identification for viscoelastic dampers have been studied in Chang and Signh (2009). A more complete numerical model to include large deformation effects in viscoelastic material can be found in Hasanpour *et al*. (2009).

Specifically, in this work, the composite connector is composed of three parts, (1) soft steel, (2) polymer material, such as rubber, and (3) conventional steel frame, and analyzed with finite element analysis. The soft steel is defined as the steel with low yield strength and high ductility. The connector, then, is bolted or welded to the column and beam. Various designs for the composite beam-column connector are conducted and compared. In the finite element analysis, effects of geometric nonlinearity, plasticity and linear viscoelasticity are included to demonstrate the energy dissipation capability of the composite connector.

2. Continuum analysis and constitutive models

In this section, we first introduce the elasticity analysis in Section 2.1, and then the viscoelasticity analysis in Section 2.2. In Section 2.3, the plasticity analysis is discussed. The continuum analysis and constitutive models serve as the theoretical foundation for later finite element numerical analysis to study the mechanical behavior of the composite beam-column connector.

2.1 Elasticity analysis

Force balance equation used in elasticity is shown in Eq. (1), where density is denoted by ρ, time t, displacement fields u, stress tensor σ and specific body force F. The symbol ∂ indicates partial derivative. Tensorial notations are not adopted for clearly presentation of the equations.

$$\rho \frac{\partial^2 u}{\partial t^2} - \nabla \cdot \sigma = \rho F, \tag{1}$$

Constitutive relationships are shown in Eq. (2) with total strain denoted by ε and inelastic strain by ε_{inel}. The colon symbol: denotes the tensorial contraction operation between fourth-order elastic constant tensor C and second-order strain tensor.

$$\sigma = C : (\varepsilon - \varepsilon_{inel}), \tag{2}$$

The strain tensor follows the following geometrical relationship with the displacement fields. The gradient operator is denoted by an upper side down triangle. A superscript T indicates a tensor transpose operation.

$$\varepsilon = \frac{1}{2}\left[(\nabla u)^T + \nabla u\right], \tag{3}$$

Combination of the all the above equations with suitable and initial boundary conditions results in the well-defined mathematical system for the elasticity problems.

2.2 Viscoelasticity analysis

When materials are viscoelastic, the force balance still obeys Eq. (1), but the constitutive relationships must be modified to reflect the nature of time dependence. The standard linear solid model is adopted, as follows

$$\sigma = Tr(K)(\varepsilon - \varepsilon_{inel})I + 2G\left(\varepsilon - \frac{1}{3}Tr(\varepsilon - \varepsilon_0)I\right) + 2Gq, \tag{4}$$

Here the bulk modulus is K, shear modulus G. The symbol Tr denotes the tensorial trace operator to sum up the diagonal terms, and second order identity tensor is denoted as I. The time dependence is embedded in the internal variable q in the above equation, and its evolution is governed by

$$\frac{\partial q}{\partial t}+\frac{1}{\tau}q=\frac{\partial}{\partial t}\left(\varepsilon-\frac{1}{3}Tr(\varepsilon-\varepsilon_0)I\right), \tag{5}$$

The relaxation time constant τ is a material parameter. The standard linear solid requires three parameters, bulk modulus K, shear modulus G and the time constant τ. For rubbery materials, their loss tangent, i.e., tan δ, is about 0.2 (Lakes 2009). It is known that the standard linear solid model predicts the following frequency dependence for tangent delta when the other relaxation time constant is $\tau/2$.

$$\tan\delta=\frac{\omega\tau}{2+\omega^2\tau^2}. \tag{6}$$

With the assumption of τ = 0.2 seconds, the loss tangent versus frequency is plotted in Fig. 1. As can be seen the chosen time constant produces loss tangent around 0.2 in the low frequency range. Hence, throughout our analysis here, we use τ = 0.2 seconds to describe the viscoelastic strength of rubbery materials. For bulk modulus, one can calculate it from Young's modulus, E, and shear modulus, G, as follows.

$$K=\frac{EG}{3(3G-E)} \tag{7}$$

The above relationship is only valid for isotropic rubber materials.

2.3 Plasticity analysis

When materials are deformed into their plastic range, the associated flow rule is adopted in the present analysis, and the strain rate is determined from the yield function as follows.

$$\dot{\varepsilon}_p=\lambda\frac{\partial F}{\partial\sigma}, \tag{8}$$

where the von Mises type yield function is defined by

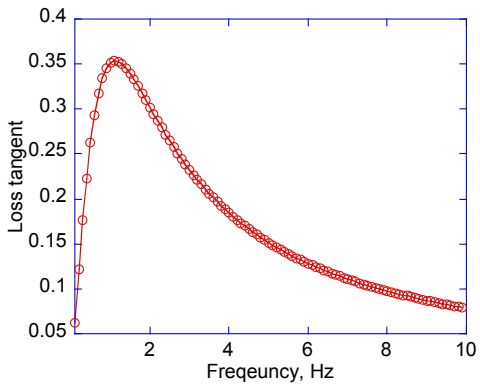

Fig. 1 Loss tangnet of rubbery materials according to Eq. (6) with the relaxation time constant 0.2 seconds

$$F = \sigma_{mises} - \sigma_{ys}. \tag{9}$$

The parameter λ is calculated from the yield function differentiated by stress (Lubliner 1990). The yield strength evolves with deformation as follows.

$$\sigma_{ys} = \sigma_{ys0} + \sigma_h, \tag{10}$$

The initial yield strength σ_{ys0} = 130 MPa, and the hardening function σ_h = 200 MPa is assumed to be independent of strain, which is commonly used in modeling steel. For standard plasticity calculations, the isotropic hardening rule is applied, i.e., for Figs. 5, 6 and 7, as well as Tables 2 and 3. For comparisons, kinematic hardening, with a tangent modulus of 2 GPa, is considered in quasi-static loading cases, as shown in Figs. 8 and 9. In addition, the elastic-perfectly plastic model is also adopted to compare the different effects on the plasticity model choice. In our chosen plastic model, the strain rate effects are neglected since only low frequency responses are considered in the present work.

Table 1 Material parameters used in the numerical calculations

	Young's modulus GPa	Poisson's ratio	Density kg/m^3	Other properties
Rubber	0.1	0.49	1,000	Relaxation time: 0.2 seconds
Soft steel	200	0.33	7,900	Yield strength: 130 MPa Hardening stress: 200 MPa Kinematic tangent modulus: 2 GPa
Steel	10,000	0.33	100,000	Assumed to be rigid

Table 2 Energy dissipation ratios for various designs

W_d/W_s	Steel	Composite 1	Composite 2	Composite 3	Composite 1-1	Composite 1-2	Composite 1-3
Shear	0.523	0.713	0.570	0.623	0.556	0.555	0.544
Com-pression	0.679	0.488	0.526	0.598	0.521	0.550	0.567
Bending	0.575	0.480	0.443	0.480	0.464	0.466	0.469

Table 3 Loss tangent for various designs

Loss tangent	Steel	Composite 1	Composite 2	Composite 3	Composite 1-1	Composite 1-2	Composite 1-3
Shear	0.333	0.454	0.369	0.397	0.354	0.353	0.346
Compression	0.433	0.311	0.335	0.381	0.332	0.350	0.361
Bending	0.366	0.305	0.282	0.306	0.296	0.296	0.298

3. Finite element details

The schematic of the physical model of the composite connector, as a whole, is shown in Fig. 2. The connector without the polymer inclusions is shown in Fig. 2(a), and that with the inclusions in Fig. 2(b). In the figures, the orange color indicates the polymer material. The ring-like parts are the soft steel which has low yield strength. In order to reduce computation load, the models for the finite element analysis are shown in Figs. 3(a)-(b) for loading condition and mesh, respectively. The height of the model is about 300 mm, and the figures are drawn to the scale. In the analysis, we treat the models as a block of material and applied shear, compressive force and bending

(a) (b)

Fig. 2 Schematics of the connector (a) without polymer; and (b) with polymer (orange color)

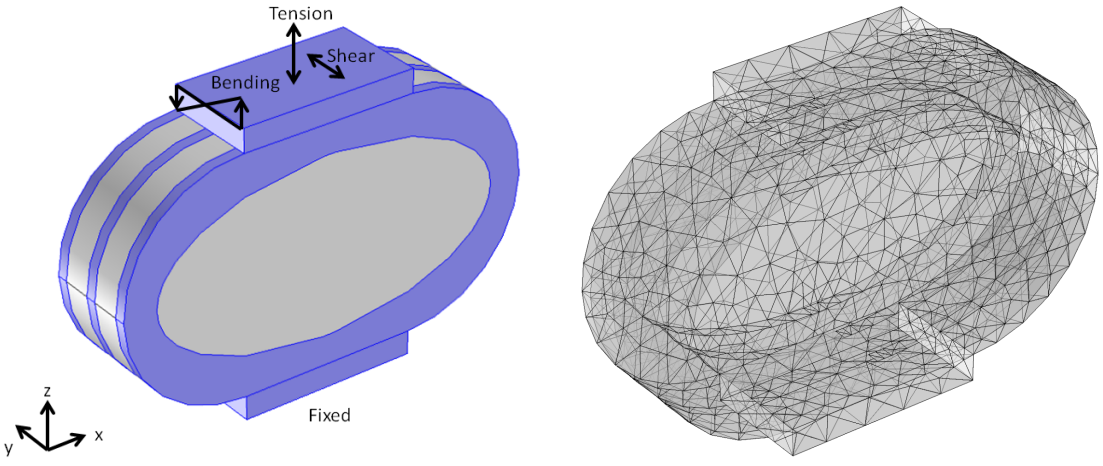

(a) (b)

Fig. 3 (a) The finite element model with indications of loading conditions; and (b) the mesh used in the numerical analysis. All loading is distributed on the whole surface of the top block. Blue color indicates the soft steel

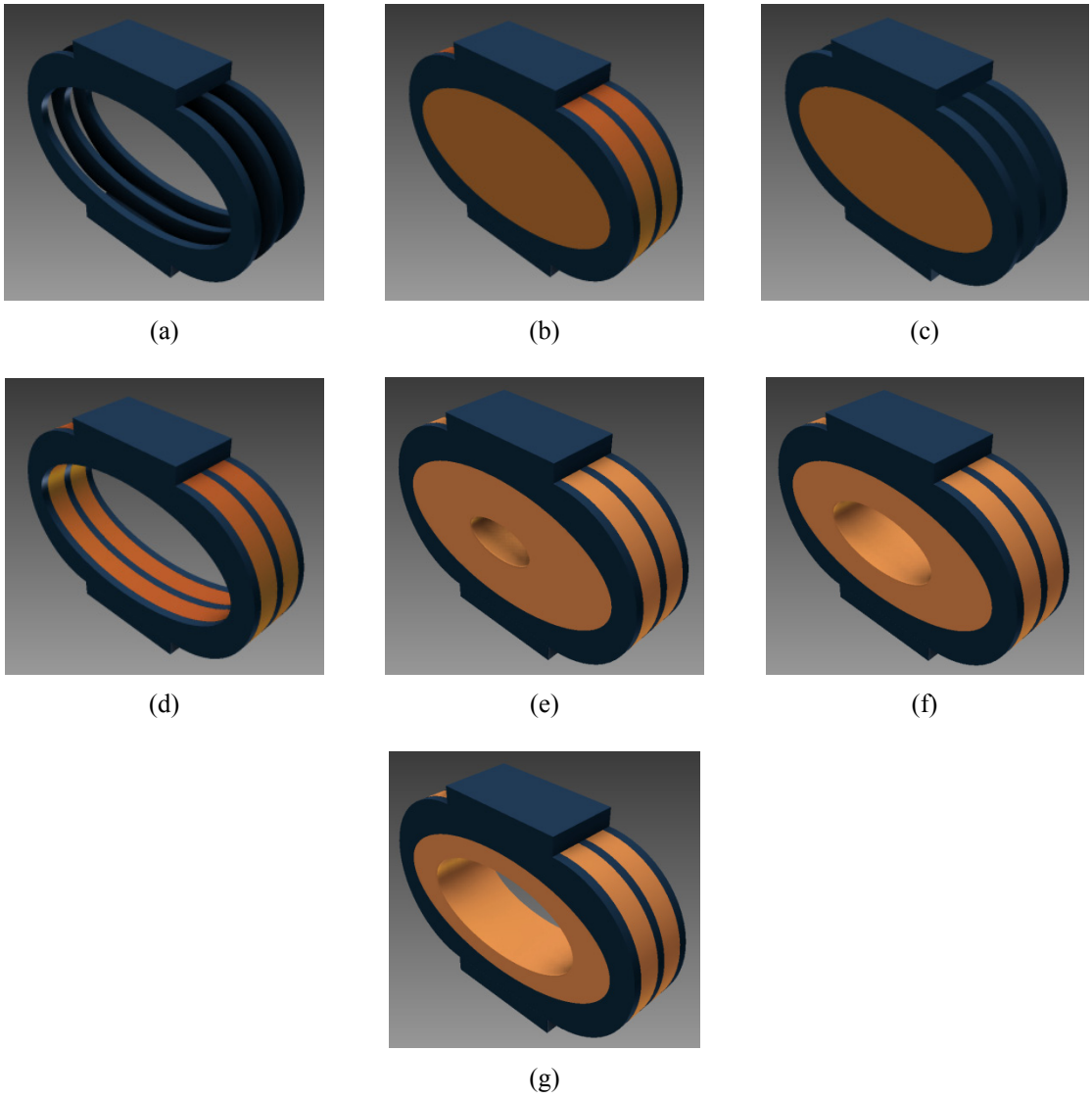

Fig. 4 Various designs for the arrangement of the polymer: (a) soft steel only (no polymer); (b) composite-1; (c) composite-2; (d) composite-3; (e) composite-1-1; (f) composite-1-2; (g) composite-1-3

moment on the top and bottom plates of the models. Furthermore, in Fig. 4, seven different designs are shown, and their difference is the amount of polymer materials used in the connector. The labels, “Steel”, “Composite-1”, “Composite-2”, “Composite-3”, “Composite-1-1”, “Composite-1-2”, “Composite-1-3” are designated for various geometrical designs in Fig. 4. The “Steel” model does not contain any polymer material, “Composite-1” model is fully filled in the plates, “Composite-2” contains polymer only in the whole core/hollow region, and “Composite-3” contains polymer between the plates only. The “Composite-1-1”, “Composite-1-2”, “Composite-1-3” follow the “Composite-1” model, but with three different size of the holes in the central region.

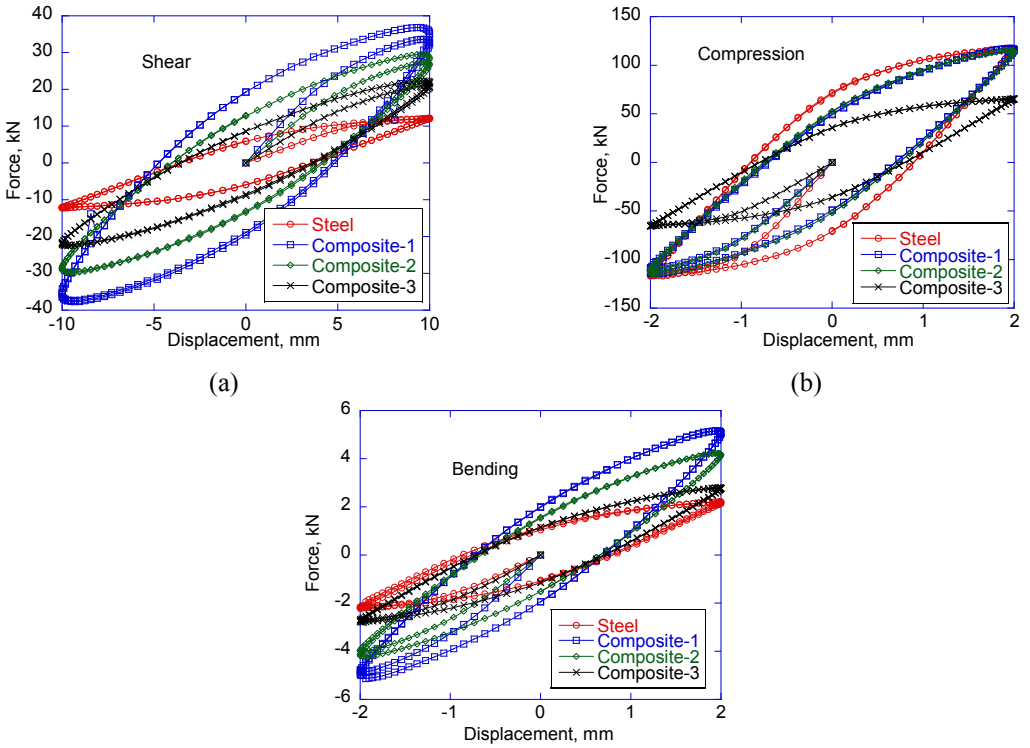

Fig. 5 Under cyclic loading (1 Hz), the force-displacement relationship of the connectors (Steel, Composite-1, Composite-2 and Composite-3) under (a) shear mode; (b) compression mode; and (c) bending mode

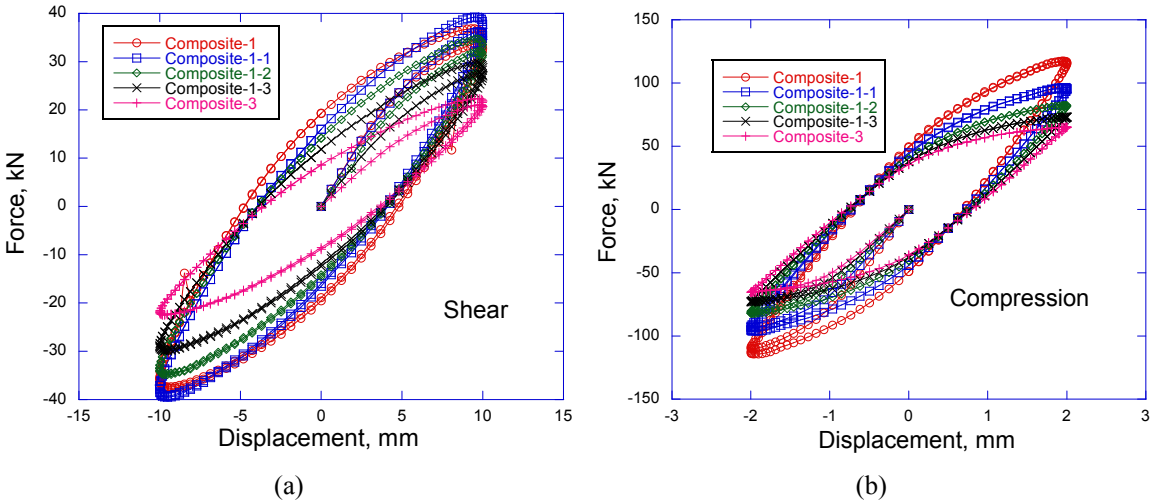

Fig. 6 Under cyclic loading (1 Hz), the force-displacement relationship of the connectors (Composite-1, Composite-1-1, Composite-1-2, Composite-1-3 and Composite-3) under (a) shear mode; (b) compression mode; and (c) bending mode

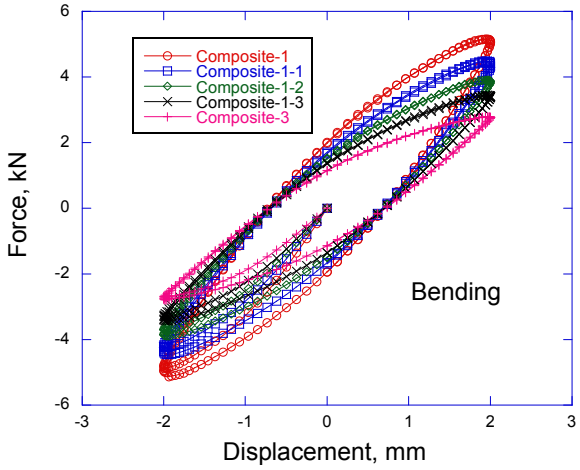

(c)

Fig. 6 Continued

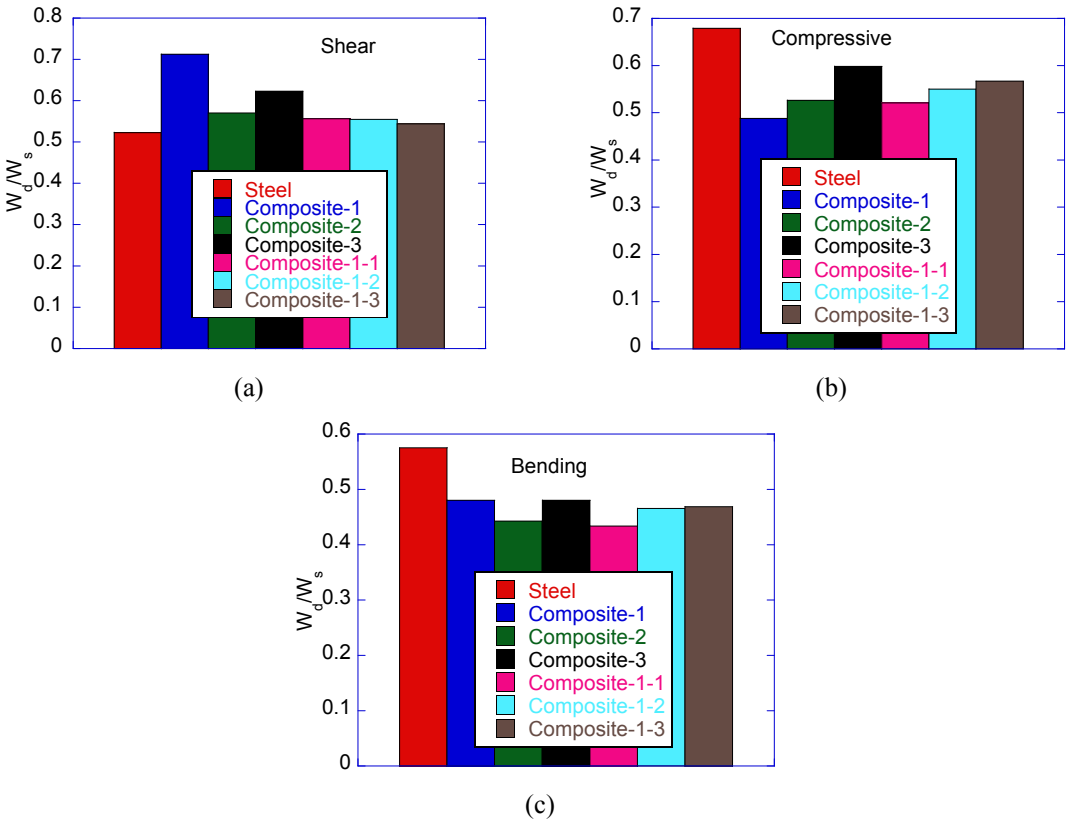

(a) (b)

(c)

Fig. 7 Energy dissipation estimation of all models for (a) shear deformation; (b) compression deformation; and (c) bending deformation

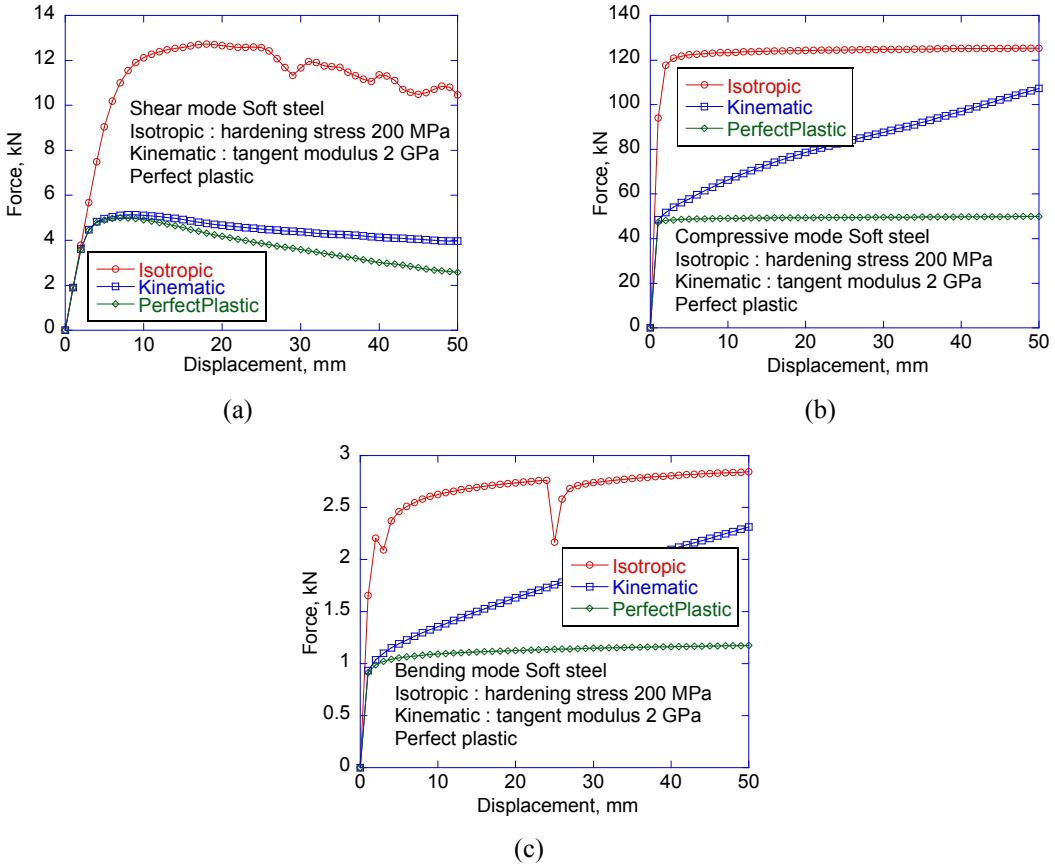

Fig. 8 Under quasi-static loading condition, the force-displacement relationship of the beam-column connector with soft steel only (no polymer) under (a) shear mode; (b) compression mode; and (c) bending mode

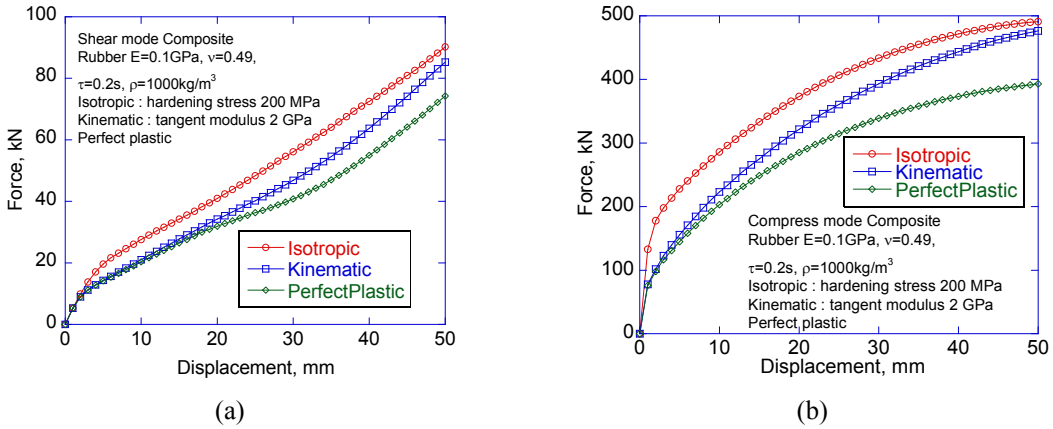

Fig. 9 Under quasi-static loading condition, the force-displacement relationship of the composite beam-column connector under (a) shear mode; (b) compression mode; and (c) bending mode

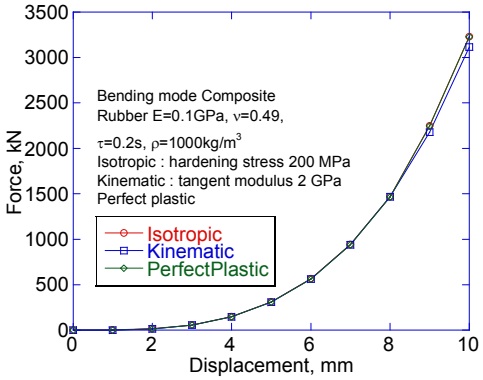

(c)

Fig. 9 Continued

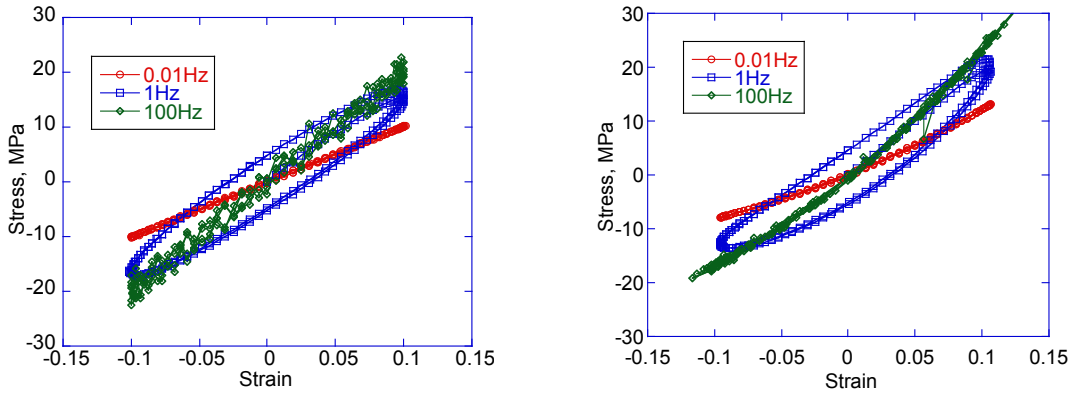

(a) (b)

Fig. 10 Stress-strain curves of rubbery material under uniaxial deformation with (a) geometric linearity; and (b) geometric nonlinearity

The three-dimensional mechanical analysis is conducted by using the finite element method with the commercial software (COMSOL Inc. 2013). If stress is large, the low-yield steel is modeled with a standard plasticity constitution that includes hardening effects, as described in Section 2.3. Otherwise, elasticity model is adopted to calculate the linear behavior of the steel. The polymer material is modeled as the standard linear solid with a relaxation time constant 0.2 seconds for its viscoelastic behavior, as described in Section 2.2. In general, rubbery materials have a loss tangent of 0.2 in the linear viscoelastic regime (Lakes 2009). The parameters in the standard linear solid model used here are so chosen to reconstruct the loss tangent in the low frequency regime. Furthermore, the focus of present study is to estimate energy dissipation capacity of the connector in the moderate deformation ranges. Hence, nonlinear elasticity constitutive models, such as the Neo-Hookean or Mooney-Rivlin models, are not included in the current analysis. Geometric nonlinearity is included in our three-dimensional finite element analysis, and its effects are discussed along with Fig. 10. Mesh density was sufficiently high to

ensure accuracy. In the analysis, linear elements were adopted. Detailed material parameters are shown in Table 1.

4. Results and discussions

Under sinusoidal displacement loading with a frequency of 1 Hz, the finite element results of Fig. 4 are shown in Figs. 5, 6 and 7 for the shear, compression and bending deformation modes. In Fig. 5, the force-displacement curves of the four designs, i.e., labeled as the "Steel", "Composite-1", "Compsoite-2" and "Composite-3" cases, are shown. The results of the shear, compression and bending mode are, respectively shown in Figs. 5(a)-(c). Similarly, in Fig. 6, the force-displacement curves of the model "Composite-1", "Composite-1-1", "Composite-1-2", "Composite-1-3" and "Composite-3" are plotted. And, Figs. 6(a)-(c), respectively, show the results of the shear, compression and bending mode.

From the three figures, it can be seen that when plasticity is not involved, i.e., in the linear regime, the hysteresis curve under sinusoidal loading shows an elliptical shape, which is a typical response of the linear viscoelastic materials, and the stress-strain curves are called as the Lissajous curves in the viscoelasticity community. The enclosed area of the ellipse is proportional to the energy dissipation capability of the material. Since stress and strain distributions in the connector are not uniform, we report the load-displacement curves to delineate the overall response of the connector. The load and displacement are obtained from the center of the top surface of the top plate (Fig. 3(b)), that is made of conventional steel, as oppose to the soft steel used in the ring. Since the top steel plate is assumed to be rigid, i.e., with a very large elastic constant, the load and displacement everywhere on the top block are roughly the same. As a remark, if the material is purely elastic, the force-displacement curves would appear as a straight, inclined line, indicating no energy dissipation capabilities.

It can be seen in Fig. 5(a) that the "Compoiste-1" and "Composite-2" case behave linearly under shear mode. However, the "Steel" model exhibits plastic deformation at maximum displacement, as the hysteresis becomes non-elliptical. The "Composite-3" case also shows a slight plastic deformation. The rationale for the stress redistributions in these cases are due to more polymer material to dilute stress in the soft steel. Furthermore, the "Composite-1" model shows the largest enclosed area, indicating its energy dissipation capacity is the highest. The increase of the energy dissipation is the combination of the deformation mode and the use of polymer. Under the compression mode, Fig. 5(a) shows all models are deformed plastically. From Fig. 5, it can be seen that, for the shear and bending mode, the more use of polymer, the higher resistant force can be obtained (under he same magnitude of deformation). However, for the compression mode, the "Composite-3" case shows the lowest resistant force.

For all the tested deformation modes, it can be seen in Fig. 6 that the "Composite-1-1", "Composite-1-2" and "Composite1-3" cases are bounded by the "Composite-1" and "Composite-3" cases. In other words, the later cases serve as the upper and lower bounds. The reduction of the resistant force exerted by the connector is proportional to the size of the hole in the center of the model. The larger the hole is, more reduction on the resistant force can be obtained. The lower limit case is the "Compoiste-3" model, and the upper limit case is the "Composite-1" model. These results are physically expected. But, through the finite element calculations, we demonstrate that the overall properties of the connector can be tailored to any design requests.

To summarize the results in Figs. 5 and 6, the energy ratio between dissipated energy W_d and

stored energy *Ws* are calculated and shown in Fig. 7. The shear, compression and bending mode are, respectively, shown in Figs. 7(a)-(c). It can be seen that under different deformation mode, different design is needed to obtain highest energy dissipation capability. The energy dissipation ratio is also shown in Table 2 for detailed numeric comparisons. Since in the composite the stress distribution is not uniform, we adopt the energy dissipation ratio as an indicator to describe the damping capability of the connector. Use of only low-yield steel without polymer may not provide the best energy dissipation capability for some deformation mode. Instead, the Composite-1 model shows the highest energy dissipation ratio due to the use of polymer material and the arrangement of the geometry. The geometry may alter the stress distributions in the connector, hence increases the energy dissipation ratio.

Furthermore, in order to compare with conventional linear viscoelastic materials, the dissipated energy ratio can be converted to loss tangent (i.e., tan δ) of the material as follows.

$$\frac{W_d}{W_s} = \frac{\pi}{2}\tan\delta. \tag{11}$$

The converted loss tangent is shown in Table 3 for all models. Since some models are deformed plastically, the conversion represents an overall estimation of the loss tangent as if the material were a linear viscoelastic type. In the connector, energy dissipation may be achieved by polymer's viscoelasticity, as well as plastic deformation of the soft steel.

Under compression, the force-displacement curves of the all cases are shown in Figs. 5(b) and 6(b). In this loading condition, the low-yield steel only model shows the highest energy dissipation ratio, as summarized in Fig. 7(b). Since the significant bent in the force-displacement curves, the low-yield steel is largely plastically deformed for the steel only model. Under this loading condition, adding polymer materials would reduce the stress in the steel, and hence the energy ratio is smaller. However, for shear mode, the "Steel" model shows the lowest energy dissipation.

When the connector is subjected to bending, the force versus displacement curves are shown in Figs. 5(c) and 6(c). The bending is applied by assuming a linear distribution of force on the top and bottom plates, and hence the force and displacement are referred to the maximum force in the linear distributed load, and corresponding displacement at the node. From Fig. 7(c), it can be seen that the "Steel" model also shows the largest energy dissipation ratio. Adding the rubbery material may not enhance the damping due to the amount of damping from the polymer is less than the damping from plastic deformation.

The "Steel" model consists of no polymer, but, in some cases, it exhibits larger damping than the cases with polymer. The rationale for this observation is because the plastic deformation of soft steel may provide high energy dissipation capacity. In order to put the soft steel in large plastic deformation, the surrounding rubbery materials need to be removed. However, there are two aspects that need to be noted. One is this observation is not for all deformation modes, hence when the connector is under complex stress state, its energy dissipation capability may not be superior than that of composite connector. The second aspect is that the large energy dissipation of the "Steel" model is obtained at the expense of severe plastic deformation. It is known that plastic deformation causes strain hardening through increase of dislocation density. Consequently, the ductility of plastically deformed steel is largely reduced due to damage accumulation. Therefore, even though the "Steel" model may exhibit high energy dissipation capacity, it is put in an irreversible process under every loading cycle. Ultimately, the connector may exhibit brittle failure. On the contrary, the composite connector exhibits damping from the viscoelastic polymer, and less

degrees of plastic deformation in soft steel. Therefore, the composite may exhibit longer life than the soft steel only connector.

All of the abovementioned discussion focus on the geometric nonlinearity and plastic deformation in soft steel. However, when the loading is in the linear regime, the damping enhancement of the connector is achieved through the viscoelastic polymer. In the linear regime, the loss tangent of steel is on the order of 10^{-6} in terms of loss tangent, but that of the rubbery material is on the order of 10^{-1} (Lakes 2009). The overall loss tangent of the connector is dominated by the polymer inclusions and geometry. Therefore, in the linear behavior, the connector exhibits larger damping capability than that of pure steel. We remark that damping also may arise from the interfaces between the connector and beam or column due to friction in the bolted joints or welds.

In addition to the cyclic loading to evaluate the mechanical properties of the connector, Figs. 8 and 9 show the quasi-static load-displacement curves of the "Steel" and "Composite-1" connector, respectively. In both figures, the shear deformation mode is shown in (a), compression mode in (b) and bending mode in (c). It can be seen that the kinematic hardening model predicts similar results as the elastic-perfectly plastic model for the shear mode in the small displacement regime. The kinematic model is a good candidate for modeling the Bauschinger effects, and in our future work the unloading simulations are to be performed to test the Bauschinger effects on the composite connector. Furthermore, the overall hardening behavior is significantly improved for the composite connector with polymer. In particular, for the "Steel" model, the isotropic hardening rule shows no overall hardening effects under the shear mode. In addition, the resistant force of the polymer-embedded connector is largely enhanced.

It is known that the area underneath the quasi-static stress-strain curve is called uniaxial toughness of the material, a combinatory measure of the strength and ductility of the material. Since, in the current computer simulations, the fracture of the connectors cannot be modeled, the end points of the force-displacement curves cannot be determined by calculations. However, Figs. 8 and 9 serve a purpose to delineate the plastic behavior of the connector with three plasticity models, i.e., the isotropic hardening model, kinematic hardening model and elastic-perfectly plastic model. It is emphasized that the isotropic hardening model is adopted in the analysis for Figs. 5, 6 and 7.

In order to clearly demonstrate the effects of geometric nonlinearity, Figs. 10(a)-(b) show the viscoelastic rubbery material under uniaxial deformation with the geometric linear and nonlinear assumption, respectively. In the finite element analysis, solid elements and other types can be treated with geometric nonlinearity such that the equilibrium equations are satisfied in the deformed geometry; not the undeformed geometry as the geometric linearity assumed (COMSOL Inc. 2013). As can be seen from the figure, the geometric linearity always produce inclined straight stress-strain curves. Under large deformation, the specimen changes shape, and geometric nonlinearity ensures the equilibrium equations are satisfied with the consideration of shape changes. Hence, stress-strain curves are nonlinear under geometric nonlinear assumption. However, this nonlinear effects cannot completely capture the constitutive relationships in the nonlinear elasticity models, such as the hyperelastic models, for rubbery materials. In modeling the behavior of rubbery materials, the Neo-Hookean or Mooney-Rivlin constitutive relationships are typically adopted (Belytschko *et al*. 2000). The hyperelastic models not only consider the effect of changes in geometry, but also include changes in material properties. In this work, geometric nonlinearity is included with viscoelastic effects, and the damping capability of the novel connector, modeled by the generalized Maxwell-Voigt model, is demonstrated. It is currently under study to combine

viscoelastic and hyperelastic material models to more realistically model the behavior of the beam-column connector. However, it is noted that hyperelastic models are adopted for modeling deformation of rubbery materials up to 500% elongation or more. In the beam-column geometry, it is unlikely that the polymer phase can be deformed up to that level of strain. However, the inclusion of hyperelastic model in the future work may still provide more realistic modeling results.

5. Conclusions

The mechanical behavior of the composite beam-column connector is studied as a material block under shear, compression and bending. Its energy dissipation capability is largely enhanced due to the following several mechanisms. In the linear regime, the viscoelastic properties of polymer material increases the overall dissipation energy ratio of the composite connector about three orders of magnitudes, when compared to purely elastic properties of the steel. In the plastically deformed regime, the soft steel provides energy dissipation through plastic deformation in the expense of permanent deformation. The amount of energy dissipation depends on deformation modes, such as in the bending and compression mode, polymer materials do not enhance overall damping properties of the composite beam-column connect. However, in the shear mode, suitable choice of rubber material in its geometry may increase the energy dissipation more than having the soft steel only. In the quasi-static loading condition, the soft steel only model does not show strong overall plastic hardening with the isotropic hardening rule, while the composite connector exhibits distinctive overall hardening behavior. Finally, in reality, additional energy dissipation mechanisms may arise from friction damping due to the bolt or weld connections between the connector and its neighbors, which are currently under intensive study.

Acknowledgments

This research work was supported by the National Science Council of the Republic of China under Grant NSC 101-2221-E-006 -206.

References

Belytschko, T., Liu, W.K. and Moran, B. (2000), *Nonlinear Finite Elements for Continua and Structures*, John Wiley & Sons, New York, NY, USA.

Calado, L., Proenca, J.M., Espinha, M. and Castiglioni, C.A. (2013), "Hysteretic behavior of dissipative welded fuses for earthquake resistant composite steel and concrete frames", *Steel Compos. Struct., Int. J.*, **14**(6), 547-569.

Chang, T.-S. and Singh, M.P. (2009), "Mechanical model parameters for viscoelastic dampers", *J. Eng. Mech.*, **135**(6), 581-584.

Chen, S.J., Yeh, C.H. and Chu, J.M. (1996), "Ductile steel beam-to-column connections for seismic resistance", *ASCE J. Struct. Eng.*, **122**(11), 1292-1299.

COMSOL Inc. (2013), http://www.comsol.com

Dong, L. and Lakes, R.S. (2012), "Advanced damper with negative structural stiffness elements", *Smart Mater. Struct.*, **21**(7), 075026.

Ferreira, A.J.M, Araujo, A.L., Neves, A.M.A., Rodrigues, J.D., Carrera, E., Cinefra, M. and Soares, C.M.M.

(2013), "A finite element model using a unified formulation for the analysis of viscoelastic sandwich laminates", *Compos*.: *Part B*, **45**(1), 1258-1264.
Hasanpour, K., Ziaei-Rad, S. and Mahzoon, M. (2009), "A large deformation framework for compressible viscoelastic materials: Constitutive equations and finite element implementation", *Int*. *J*. *Plast*., **25**(6), 1154-1176.
Higashino, M. and Okamoto, S. (2006), *Response Control and Seismic Isolation of Buildings*, Taylor & Francis, New York, NY, USA.
Ibrahim, Y.E., Marshall, J. and Charney, F.A. (2007), "A visco-plastic device for seismic protection of structures", *J*. *Construct*. *Steel Res*., **63**(11), 1515-1528.
Kappos, A.J., Saiidi, M.S., Aydinoglu, M.N. and Isakovic, T. (2012), *Seismic Design and Assessment of Bridges*, Springer, Dordrecht, The Netherlands.
Kelly, J.M., Skinner, R.I. and Heine, A.J. (1972), "Mechanisms of energy absorption in special devices for use in earthquake resistant structures", *Nat*. *Soc*. *Earthq*. *Eng*., **5**(3), 63-88.
Kim, J., Ryu, J. and Chung, L. (2006), "Seismic performance of structures connected by viscoelastic dampers", *Eng*. *Struct*., **28**(2), 183-195.
Lakes, R.S. (2009), *Viscoelastic Materials*, Cambridge University Press, New York, NY, USA.
Lubliner, J. (1990), *Plasticity Theory*, Macmillan Publishing Company, New York, NY, USA.
Nashif, A.D., Jones, D.I.G. and Henderson, J.P. (1985), *Vibration Damping*, John Wiley, New York, NY, USA.
Ross, D., Ungar, E.E. and Kerwin, E.M. Jr. (1959), "Damping of plate flexural vibrations by means of viscoelastic laminate", In: (ASME Ed.) *Structural Damping*; New York, NY, USA, pp. 49-88.
Symans, M.D., Charney, F.A., Whitaker, A.S., Constantinou, M.C., Kircher, C.A., Johnson, M.W. and McNamara, R.J. (2008), "Energy dissipation systems for seismic applications: Current practice and recent developments", *J*. *Struct*. *Eng*., **134**(1), 3-21.
Taranath, B.S. (1988), *Structural Analysis and Design of Tall Buildings*, McGraw-Hill, Boston, MA, USA.
Tremblay, R., Bolduc, P., Neville, R. and DeVall, R. (2006), "Seismic testing and performance of buckling-restrained bracing systems", *Can*. *J*. *Civ*. *Eng*., **33**(2), 183-198.
Tsai, K.C., Chen, H.W., Hong, C.P. and Su, Y.F. (1993), "Design of steel triangular plate energy absorbers for seismic-resistant construction", *Earthq*. *Spectra*, **9**(3), 505-528.
Whittaker, A.S., Bertero, V.V., Thompson, C.I. and Alonso, L.J. (1991), "Seismic testing of steel plate energy dissipation devices", *Earthq*. *Spectra*, **7**(4), 563-604.
Xu, Z.D., Jia, D.H. and Zhang, X.C. (2012), "Performance tests and mathematical model considering magnetic saturation for magnetorheological damper", *J*. *Intell*. *Mater*. *Syst*. *Struct*., **23**(12), 1331-1349.
Xu, Z.D., Huang, X.H., Guo, Y.F. and Wang, S.A. (2013), "Study of the properties of a multi-dimensional earthquake isolation device for reticulated structures", *J*. *Construct*. *Steel Res*., **88**, 63-78.
Zhang, H.D. and Wang Y.F. (2012), "Energy-based numerical evaluation for seismic performance of a high-rise steel building", *Steel Compos*. *Struct*., *Int*. *J*., **13**(6), 501-519.
Zhang, X.C. and Xu, Z.D. (2012), "Testing and modeling of a CLEMR damper and its application in structural vibration reduction", *Nonlinear Dynam*., **70**(2), 1575-1588.
Zou, L., Huang, K., Rao, Y., Guo, R. and Zu, Z. (2013), "Research on isolation property of prestressed thick rubber bearings", *J*. *Vibroeng*., **15**(1), 383-394.

CC